

# 行政院國家科學委員會專題研究計畫 期中進度報告

## 一種產生高光觸媒活性的奈米 TiO<sub>2</sub> 微粒的新燃燒法(1/3)

計畫類別：個別型計畫

計畫編號：NSC94-2211-E-009-048-

執行期間：94年08月01日至95年07月31日

執行單位：國立交通大學環境工程研究所

計畫主持人：蔡春進

計畫參與人員：Andrei Onischuk

報告類型：精簡報告

報告附件：國際合作計畫研究心得報告

處理方式：本計畫可公開查詢

中 華 民 國 95 年 5 月 30 日

行政院國家科學委員會補助專題研究計畫  成果報告  
 期中進度報告

一種產生高光觸媒活性的奈米  $\text{TiO}_2$  微粒的新燃燒法(1/3)

計畫類別： 個別型計畫  整合型計畫

計畫編號：NSC 94-2211-E-009-048-

執行期間： 94年8月1日 至 95年7月31日

計畫主持人：蔡春進

共同主持人：Andrei Onischuk

成果報告類型(依經費核定清單規定繳交)： 精簡報告  完整報告

本成果報告包括以下應繳交之附件：

- 赴國外出差或研習心得報告一份
- 赴大陸地區出差或研習心得報告一份
- 出席國際學術會議心得報告及發表之論文各一份
- 國際合作研究計畫國外研究報告書一份

處理方式：除產學合作研究計畫、提升產業技術及人才培育研究計畫、  
列管計畫及下列情形者外，得立即公開查詢

涉及專利或其他智慧財產權， 一年 二年後可公開查詢

執行單位：國立交通大學環境工程研究所

中華民國 95 年 5 月 30 日

## Abstract

Titanium dioxide particles are used in the manufacture of pigments, as paper filler, catalysts, cosmetics, and to other applications. One of possible methods for production of TiO<sub>2</sub> nanoparticles is combustion of liquid titanium droplets.

Formation of metal oxide nanoparticles was studied during combustion of Al / Ti droplets moving in the air at the velocity of 10 - 300 m/s. The experimental data are reasonably described in terms of an analytical model considering diffusion of titanium oxide vapor (or Al and O<sub>2</sub>), titanium oxide crystalline shell formation, TiO<sub>2</sub> droplet burst due to the nitrogen release followed by the inner droplet pressure increase. The model predicted that the titanium oxide nucleation occurs at the distance of about 10 μm from the burning surface at the critical supersaturation  $S_{crit} \approx 3.5$ . Then the nanoparticles are driven outwards by the thermophoresis.

In this study the numerical model of liquid titanium particle combustion in air stream was also developed. The time evolution of oxygen concentration in droplet and products (Ti, TiO and TiO<sub>2</sub> vapor) in the air were calculated. The variation of droplet diameter in time due to evaporation of titanium oxides and dissolution of oxygen was taken into account. The temperature distribution in both phases was predicted. Also the nucleation and coagulation titanium dioxide was modeled and size distribution of primary and agglomerate aerosol particles was predicted,

According to our model it is possible to predict the amount and size distribution of TiO<sub>2</sub> nanoparticles produced during the liquid titanium droplet combustion at different operating conditions such as: initial droplet diameter, ambient air and initial droplet temperature, air stream velocity.

**Keywords:** combustion, TiO<sub>2</sub>, nucleation, aggregation

## 摘要

二氧化鈦用於顏料的生產、紙的填充料、觸媒、化妝品及其他的應用等。以燃燒產生 TiO<sub>2</sub> 奈米微粒是一個可行的方法。

本研究中，燃燒在空氣中移動速度介於 10-300 m/s 的 Al / Ti 液滴，來探討氧化金屬奈米微粒的形成機制。實驗的數據可用一個解析的理論推導結果來解釋，這個理論考慮了包括：鈦氧化物(或鋁氧化物)的擴散、氧化鈦晶殼的形成及二氧化鈦的破裂是因為液滴內壓力增加造成氮氣釋放所致。模式預測氧化鈦凝結發生在過飽和比 3.5 時及距離燃燒表面約 10 μm 的位置，然後奈米微粒因熱泳而被向外驅出。

在本研究中，我們也以數值方法模擬二氧化鈦液滴的燃燒，計算液滴中含氧量及空氣中的 Ti, TiO 及 TiO<sub>2</sub> 蒸氣的逐時濃度，並考慮 TiO<sub>2</sub> 揮發時液滴直徑及溶氧的變化。我們也已模擬了 TiO<sub>2</sub> 氣相及液相溫度的變化，TiO<sub>2</sub> 的核化及膠結，並預測出一次及聚結奈米 TiO<sub>2</sub> 微粒之粒徑分佈。根據模式，我們可以預測在不同初始 TiO<sub>2</sub> 液滴的直徑，初始液滴溫度，空氣速度時燃燒產生 TiO<sub>2</sub> 奈米微粒的數量及粒徑分佈。

**關鍵詞：**燃燒、二氧化鈦、核凝、膠結

## 1. INTRODUCTION

The investigations of single metal droplets combustion are inspired by both fundamental interest [1, 2] and possible applications [3]. In particular the combustion of metal powder can be an effective way of synthesis of semiconductor and ceramic oxide nanoparticles [3]. Metal powders are of interest as ingredients for high energetic formulations. Aluminum powders are added to propellants and explosives to boost their combustion enthalpy [2, 4, 5]. It has been recognized also that other metals like titanium, beryllium, zirconium can be useful as energetic additives in propellants, explosives and incendiaries [6]. In respect to these applications a single metal particle burning in air at 1 atm was selected by many researches (see, for example, [1, 7, 8]) as a simple model for theoretical and experimental study. Metal oxide nanoparticles are a product of maternal metal particle combustion. However the mechanism of nanoparticles formation is not understood completely yet, partially, due to the lack of experimental data

Titanium dioxide particles are used the manufacture of pigments, as paper filler, catalysts, cosmetics, and to other applications. On the other hand one of the ways to neutralize the dangerous compounds in the atmosphere, that can occur due to catastrophes in chemical plants, on transport, etc., can be dispersion of sufficient amount of highly active catalytic particles in the air.  $TiO_2$  nanoparticles in the anatase crystal modification exhibit excellent photo-catalytic properties. One of possible methods for production of  $TiO_2$  nanoparticles is combustion of liquid titanium droplets.

The objective of this study is to investigate the mechanism of  $TiO_2$  and  $Al_2O_3$  nanoparticle formation during combustion of  $Ti$  and  $Al$  droplets in air at atmospheric pressure. The main questions under consideration were metal oxide nanoparticle size, morphology, mobility, electric charge as well as stages of combustion of maternal droplets. Previously the formation of  $Al_2O_3$  nanoparticles were studied in [9], therefore, the present paper is more focused to the titanium droplet combustion. The goal of the present work is to investigate formation of titanium nanoparticles in combustion of  $Ti$  droplets in the air.

## 2. METHODS

### 2.1 Experimental

Metal oxide nanoparticles were formed by combustion of  $Al$  or  $Ti$  droplets moving in the air at atmospheric pressure. Two types of experiments were carried out. In the first case a single particles of diameter 100 - 350  $\mu m$  were charged into a quartz capillary together with an igniting composition. The capillary inner diameter was 0.2 cm. The igniting composition consisted of oxidizer and binder and served to ignite the particles and eject them one after another to the ambient air with the velocity of 100 - 300 cm/s. The moving burning droplet was recorded by a high speed video camera. The droplet collided at a small angle with a special glass support covered by a formval film (trade mark - "Formvar") so that the metal oxide nanoparticles were freezed at the early stage of growth. As a result the nanoparticle deposit was formed at the surface. The deposit distribution was analyzed by an optical microscope. Finally the Formvar film with deposit was detached from the surface, put to the copper electron microscopy grid, and analyzed using an Transmission Electron Microscope (TEM). The main advantage of this technique was

that the quenched deposited nanoparticles gave an insight to the earliest stages ( $10^{-4}$  msec) of particle growth. The time of droplet flight was varied by the change of distance between the capillary and the surface and was in the range between 50 - 100 ms.

The second type of combustion experiments was as follows. A small sample of pyrotechnic specimen composed by oxidizer, binder and metal powder was burned in a 20 litres reaction vessel. The size of metal powder was in the range 4 - 350  $\mu\text{m}$ . The combustion time was about a few seconds. During the combustion the burning original metal liquid particles (or "agglomerates" which were formed by merging of the original metal particles) were ejected to the gas phase. The burning droplets moved in the ambient air and generated  $\text{Al}_2\text{O}_3$  /  $\text{TiO}_2$  aerosol. From the video records we determined the droplet combustion time as 0.05 - 0.3 s and the droplet velocity about 10 - 50 cm/s. Thus, the pyrotechnical composition was used only to ignite metal particles and the main droplet combustion proceeded in the air of reaction chamber. The metal droplet combustion resulted in the metal oxide aerosol formation. This  $\text{Al}_2\text{O}_3$  /  $\text{TiO}_2$  aerosol was left in the vessel for certain time (from 1 to 20 min after combustion being terminated). Then the aerosol particles were sucked from the combustion chamber and sampled thermophoretically for the Transmission Electron Microscopy analysis and for the analysis by a video microscopy system. The TEM analysis gave information about the size and morphology of aerosol particles. The video microscope was used to observe the Brownian motion of aggregates [9] as well as motion in the electric field. In these experiments a probe of aerosol was injected to the optically accessible modified Millikan cell. Focused He-Ne laser beam passed through the cell volume. A light scattered by aerosol particles at the angle of  $90^\circ$  passed through a flat window to a microscope objective and then to a CCD camera. The objective draws an image of particles present in the illuminated volume of cell on the light sensitive CCD-matrix. The visualization field in the optical cell is  $300 \times 400 \mu\text{m}^2$  or larger. The spatial resolution of the system is near 3  $\mu\text{m}$  that allows to obtain resolved images of aggregates larger than 3  $\mu\text{m}$ . For smaller size, the aggregates are visible as spots. To create homogeneous electric field two parallel flat electrodes were installed in the cell. The distance between electrodes was 0.25 cm. The movement of the aggregates in homogeneous electric field gave the information on the electric charge and dipole moment of resolved visible aggregates.

## **2.2 Theoretical and numerical**

### *2.2.1 The Combustion process*

Experiments have shown that metal/oxygen solutions are formed in burning metal particles prior to the formation of stoichiometric oxides. The combustion process always terminates with explosion [10]. During combustion process different species are evaporated from the droplet surface. As it was shown by Heideman et al. [11] concentrations of other species are negligible in comparison with Ti, TiO and  $\text{TiO}_2$ . Molodetsky et al. [10] concluded that Ti oxidation in gas phase is insignificant. The picture of combustion process is complex including dissolution of oxygen in titanium, diffusion of dissolved oxygen into the droplet, chemical reaction, evaporation of Ti and titanium oxides, their transport in gas phase, nucleation and aggregation.

### *2.2.2 Mass transport model*

For modeling of combustion process we need to solve the standard convection-diffusion equation

$$\frac{\partial c_i}{\partial t} = D_i \nabla^2 c_i + v \nabla c_i \quad (1)$$

for all the species, namely, Ti, TiO, TiO<sub>2</sub> and O<sub>2</sub> in gas phase and atom oxygen in liquid phase. In above equation  $c_i$  is mole concentration [mol/m<sup>3</sup>] of  $i$ -th component,  $D_i$  its diffusion coefficient [m<sup>2</sup>/s],  $v$ -fluid velocity [m/s] and  $t$  is time [s]. Thus we need to write initial boundary and conditions for all the species. The problem will be solved in radial coordinate system in the beginning in the droplet of radius  $R_d$  center. So for Ti and titanium oxides we can write

$$c_{Ti}|_{t=0} = c_{TiO}|_{t=0} = c_{TiO_2}|_{t=0} = 0 \quad (2)$$

for  $r \geq R_d$ . Initial concentration of O<sub>2</sub> in gas phase can be easily found from the ideal gas equation of state.

$$c_{O_2}|_{t=0} = 0.21 \cdot \frac{P}{RT_\infty} \quad (3)$$

where  $P$  is air pressure [Pa],  $R$  gas constant [J/(molK)] and  $T_\infty$  ambient air temperature [K]

Initially there is no oxygen dissolved in liquid phase, so for  $r \leq R_d$  one can write

$$c_O|_{t=0} = 0 \quad (4)$$

The total pressure of Ti<sub>x</sub>O<sub>y</sub> vapor (consisting of Ti, TiO and TiO<sub>2</sub>) at the droplet surface ( $r=R_d$ ) can be estimated by equation

$$P_{Ti_xO_y} = 1.605 \cdot 10^{17} (34.498X + 1) \exp\left(\frac{-100600}{T_R}\right) \quad (5)$$

where  $X$  is the atom fraction of oxygen on the droplet surface in liquid phase and  $T_R$  is droplet surface temperature. Eq. (5) was obtained by interpolation of available data for stoichiometric compounds [12]. The relation between oxygen atom fraction in the liquid phase,  $X$ , and in Ti<sub>x</sub>O<sub>y</sub> vapor,  $Y$ , on the droplet surface can be estimated from Ti-O phase diagram [13]

$$Y = 0.05 + X + X^3 \quad (6)$$

The amount of species in Ti<sub>x</sub>O<sub>y</sub> vapor can be calculated by finding the minimum value of its Gibbs energy,  $G$  [J/mol]

$$G_{Ti_xO_y} = \sum_i [x_i G_i + RT(x_i \ln x_i)] \quad (7)$$

with additional conditions

$$\sum_i x_i = 1 \quad (8)$$

and

$$\frac{x_{TiO} + 2x_{TiO_2}}{x_{Ti} + 2x_{TiO} + 3x_{TiO_2}} = Y \quad (9)$$

where  $x_i$  is atom fraction of  $i$ -th component in  $Ti_xO_y$  vapor,  $G_i$  is Gibbs energy of pure component, and  $\sum_i RT(x_i \ln x_i)$  is Gibbs energy of mixing. Thermodynamic data necessary for Gibbs energy calculations were presented by Waldner and Eriksson [14].

Having boundary conditions for  $r=R_d$  for compounds containing Ti atoms now we will formulate boundary conditions for oxygen in liquid and gas phase. The flux of oxygen from the droplet surface can be calculated from the kinetic equation of oxygen dissolution in liquid titanium.

$$D_o \nabla c_o + \mathbf{v}c_o = K(c_{o,sat} - c_{o,bulk}) \quad (10)$$

where  $c_{o,sat}$  is saturation concentration of oxygen in titanium and  $c_{o,bulk}$  is the oxygen concentration in bulk of liquid phase in our case in the droplet center) The mass transfer coefficient between gas and liquid phase,  $K$ , can be found from Sherwood number,  $Sh$ .

$$Sh = \frac{K \cdot 2R_d}{D_o} \quad (11)$$

For liquid droplet Sherwood number is equal  $Sh=6.6$  [15].

The last boundary condition on the droplet surface we find from the oxygen balance on the interphase surface

$$2(D_{O_2} \nabla c_{O_2} + \mathbf{v}c_{O_2}) = (D_o \nabla c_o + \mathbf{v}c_o) + (D_{TiO} \nabla c_{TiO} + \mathbf{v}c_{TiO}) + 2(D_{TiO_2} \nabla c_{TiO_2} + \mathbf{v}c_{TiO_2}) \quad (12)$$

The droplet radius is varying in time due to evaporation of combustion products and dissolution of oxygen. The volume of liquid phase per one mole of titanium as a function of mean atom fraction of oxygen in droplet,  $V_{Ti}$  [ $m^3$ ], can be written as

$$V_{Ti} = 1.43 \cdot 10^{-9} \exp\left(\frac{\bar{X}}{0.102}\right) + 1.07 \cdot 10^{-5} \quad (13)$$

So the temporary radius of droplet is equal to

$$R_d(t) = \left[ \frac{3}{4\pi} N_{Ti}(t) V_{Ti}(\bar{X}(t)) \right]^{1/3} \quad (14)$$

where  $N_{Ti}(t)$  is temporary number of Ti moles in droplet.

### 2.2.3 Heat transfer

Temperature distributions in both, liquid and gas phase were calculated using convective-diffusive equation of heat transfer

$$\frac{\partial}{\partial t}(\rho E) + \nabla(\mathbf{v}(\rho E + P)) = \nabla(\chi \nabla T - \sum_i H_i \mathbf{J}_i) \quad (15)$$

where  $E$  [J/kg] is total energy,

$$E = H - \frac{P}{\rho} + \frac{v^2}{2} \quad (16)$$

$\chi$  [m<sup>2</sup>/s) is thermal conductivity,  $\rho$  [kg/m<sup>3</sup>] is density  $H$  [J/kg] is enthalpy and  $\mathbf{J}_i$  is diffusive flux of specie  $i$ .

The heat balance on the droplet surface can be written as

$$\lambda_l \nabla T_l \Big|_{r=R_d} + \lambda_g \nabla T_g \Big|_{r=R_d} + \zeta \sigma T^4 \Big|_{r=R_d} = \sum_i \Delta q_i \mathbf{J}_i \Big|_{r=R_d} \quad (17)$$

where  $\lambda$  [W/(mK)] is heat transfer coefficient,  $\Delta q_i$  [J/mol] is the heat release of specie  $i$  according to reaction and evaporation,  $\zeta$  [-] is a emissivity coefficient, and  $\sigma$  [W/(m<sup>2</sup>K<sup>4</sup>)] is Stefan-Boltzmann constant. Subscripts  $l$  and  $g$  refer to liquid and gas phase. It was also assumed that there's no temperature jump on the droplet surface

$$T_l \Big|_{r=R_d} = T_g \Big|_{r=R_d} \quad (18)$$

#### 2.2.4 Nucleation and coagulation

The rate of change of particle size distribution due to nucleation coagulation and condensation can be described by discrete dynamical equation [16]

$$\frac{dN_k}{dt} = \frac{1}{2} \sum_{j=1}^{k-1} \beta_{k-j,j} N_{k-j} N_j - N_k \sum_{j=1}^{\infty} \beta_{k,j} N_j + J(t) \delta(k) + \beta_{1,k-1} N_1 N_{k-1} - \beta_{1,k} N_1 N_k \quad (19)$$

where  $N_k$  [1/m<sup>3</sup>] is time dependent number concentration of particles of volume  $v_k$  [m<sup>3</sup>],  $\beta$  [m<sup>3</sup>/s] is coagulation kernel of two colliding particles,  $J(t)$  is the nucleation rate and  $\delta$  is the Kronecker's delta. The nucleation rate  $J$  [1/(m<sup>3</sup>s)] can be written as [17]

$$J = \frac{\beta_{ij} n_s^2 S}{12} \sqrt{\frac{\Theta}{2\pi}} \exp\left(\Theta - \frac{4\Theta^3}{27 \ln^2 S}\right) \quad (20)$$

where  $n_s$  [1/m<sup>3</sup>] is the equilibrium saturation monomer concentration,  $S$  [-] is saturation ratio. The dimensionless surface tension is  $\theta$  is given by

$$\Theta = \frac{\sigma s_1}{kT} \quad (21)$$

where  $s_1$  [m<sup>2</sup>] is monomer surface area and  $\sigma$  [N/m] is surface tension.

The collision kernel for nucleation can be expressed as

$$\beta_{ij} = \left(\frac{3v_1}{4\pi}\right)^{1/6} + \sqrt{\frac{6kT}{\rho_p} \left(\frac{1}{i} + \frac{1}{j}\right) (i^{1/3} + j^{1/3})^2} \quad (22)$$

where  $v_1$  [m<sup>3</sup>] is the monomer volume and  $\rho_p$  [kg/m<sup>3</sup>] is particle density. For coagulation the Fuchs interpolation function was used [18]. Furthermore, the effect of aggregate structure on the collision kernel is incorporated by replacing primary particle diameter  $d_{p,i}$  with so-called collision

diameter  $d_{c,i}$  [19]

$$\beta_{ij} = 2\pi(D_i + D_j)(d_{c,i} + d_{c,j}) \left[ \frac{d_{c,i} + d_{c,j}}{d_{c,i} + d_{c,j} + 2g_{i,j}} + \frac{8(D_i + D_j)}{c_{i,j}(d_{c,i} + d_{c,j})} \right]^{-1} \quad (23)$$

where  $D_i$  [ $\text{m}^2/\text{s}$ ] is the diffusion coefficient of an aggregate of size  $i$  based on the collision diameter,  $g_{i,j}$  [ $\text{m}$ ] is the transition parameter and  $c_{i,j}$  [ $\text{m/s}$ ] has units of velocity [ $\text{m/s}$ ] as defined by Seinfeld [9]. The collision diameter of an aggregate was given by Kruis et al. [20].

$$d_{c,i} = d_{p,i} \left( \frac{v_i}{v_{p,i}} \right)^{1/D_f} \quad (24)$$

and

$$d_{p,i} = \frac{6v_i}{s_i} \quad (25)$$

where  $v_{p,i}$  [ $\text{m}^3$ ] is the volume of spherical primary particle and  $D_f$  is mass fractal dimension (varying from 1 to 3). As a first approximation the constant value  $D_f=1.8$  can be used [20,21].

Parallel to nucleation and coagulation process the particle transport was calculated using standard convective-diffusive equation [22].

$$\frac{\partial N_i}{\partial t} = \nabla(D_i \nabla N_i) - \nabla(\mathbf{v} N_i) \quad (26)$$

where  $v$  [ $\text{m/s}$ ] is gas velocity.

### 3. RESULTS AND DISCUSSION

The magnified image of the burning *Al* droplet is shown in Fig. 1. One can see clear the detached reaction zone (seen as a halo) where the aluminum oxide nanoparticles are formed in the reaction between *Al* vapor and atmospheric oxygen. In some cases very large aggregates with the diameter from a few tens to a few hundred microns were observed in the "smoke tale" (Fig. 1a, 2a, 3a). One can see also an oxide cap on the surface of *Al* droplet (Fig. 1b). We found that the radius of the reaction zone is a function of the drop radius. The ratio between the radius of the droplet and that of the halo is presented in Fig. 4 for the droplets moving with the velocity of about 1000 cm/s. Fig. 5 shows the oxide smoke tail formed during the combustion of *Ti* droplet. One can see that there is no detached reaction zone (as in contrast to the case of *Al*); the titanium oxide nanoparticles are formed just near the droplet surface.

To make an insight to the initial stages of oxide nanoparticle formation the combustion process was frozen by the collision of burning droplet with a glass surface at a small angle. Figs. 2a and 3a show optical microscope images of deposits formed by deposition of *Al* and *Ti* droplets and density profiles for these images. The deposit density profiles for  $\text{Al}_2\text{O}_3$  and  $\text{TiO}_2$  (Figs. 2b and 3b) are quite different. In the case of  $\text{Al}_2\text{O}_3$  two maximums are clear seen corresponding to nanoparticles from the detached reaction zone (see also Fig. 1); in the case of  $\text{TiO}_2$  there is a bell-shape density distribution in the central part of the deposit indicating to the fact that the reaction with oxygen is attached to the droplet surface. TEM images for  $\text{TiO}_2$  deposit are shown in Fig. 6. One can see that near the droplet surface there are single particles and relatively small

aggregates. On the other hand, there are very long chain-like aerosol aggregates in the smoke tail.

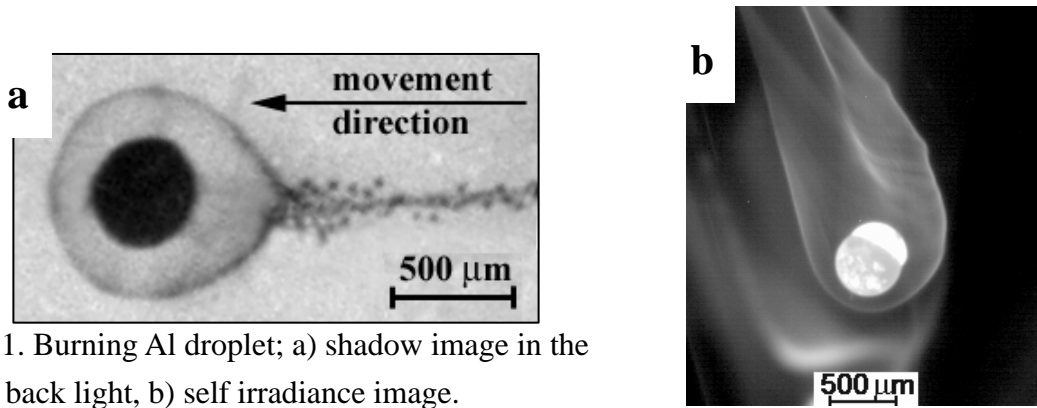


Fig. 1. Burning Al droplet; a) shadow image in the blue back light, b) self irradiance image.

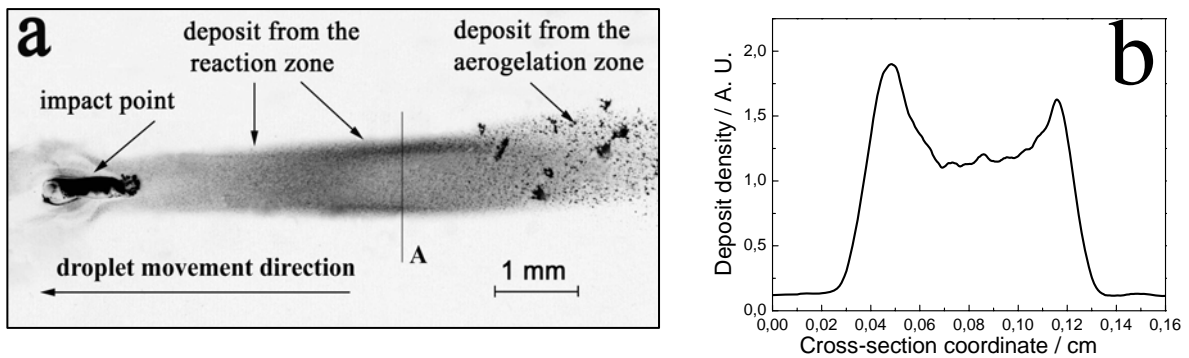


Fig. 2. (a) Optical microscope image of a deposit formed at the glass surface due to the impact of burning Al droplet at small angle; (b) density profile of the deposit at location A. The diameter of maternal droplet is 300  $\mu\text{m}$ .

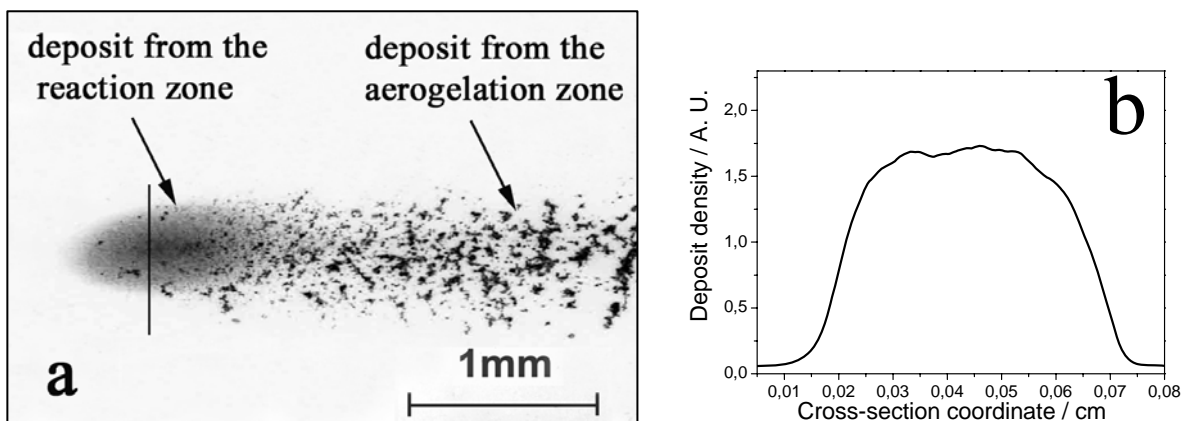


Fig. 3. (a) Optical microscope image of a deposit formed at the surface due to the impact of burning Ti droplet at small angle; (b) density profile of the Ti deposit from the reaction zone. The diameter of maternal droplet is 330  $\mu\text{m}$ .

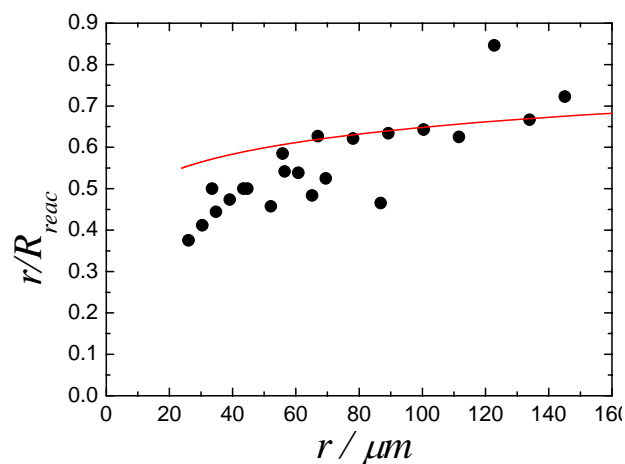


Fig. 4. Ratio between the radius of halo and that of the droplet vs. radius of Al droplet (symbols). The air counter flow velocity is about 1000 cm/s. Solid line is the solution of Eqs. (43, 44).

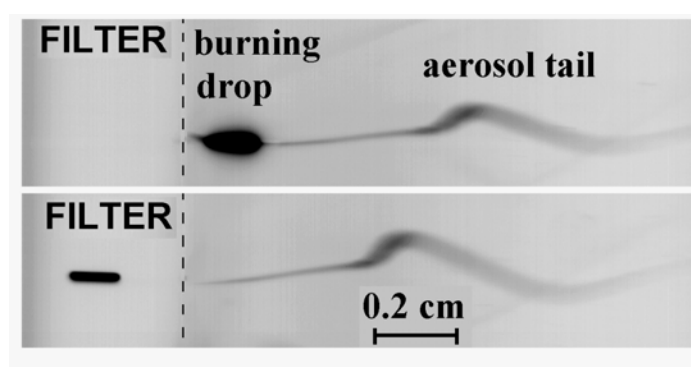


Fig. 5. Two consecutive frames (negatives) of the burning Ti droplet in the 90° scattered light. The initial droplet diameter is 200  $\mu\text{m}$ . Frame frequency is 1 KHz, frame duration is 0.9 ms. The left side of the frame is filtered to avoid the droplet over irradiance (to measure the droplet diameter).

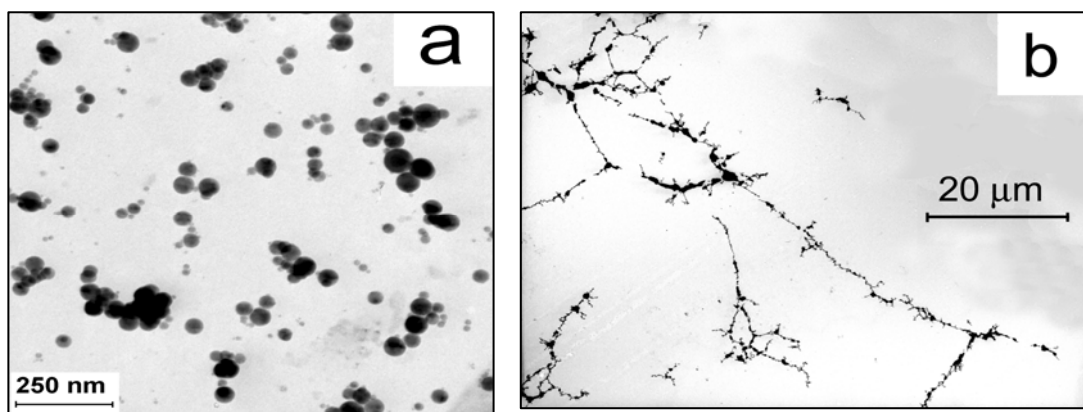


Fig. 6. TEM images of TiO<sub>2</sub> nanoparticles deposited on the substrate by combustion of single Ti droplet: a - from the reaction zone, b - from the aerogelation zone.

The calculations were performed for combustion titanium particle of diameter 240  $\mu\text{m}$  with initial temperature 2000°C to compare the results with available experimental data [10]. We have used the CFD package Fluent 6.1. To save computational time 2D calculations were performed.

The size of computational domain was  $3000\ \mu\text{m} \times 3000\ \mu\text{m}$  with 10,000 nodes and the droplet was placed centrally. The particle was combusted in the air stream of averaged velocity 2 m/s. The time for calculations of droplet combustion was chosen to be 250 ms, what corresponds to experimental data.

Fig. 7 shows the history of average and surface oxygen concentration in the droplet. The data for average concentration agrees well with experimental data. Fig. 8 and Fig. 9 present the temperature and heat release history of titanium droplet. These results agree qualitatively with experimental data for period of time from 0 to 150 ms. Although later the decrease of both heat release and particle temperature were observed experimentally, while our model doesn't predict this phenomena, which are believed to be responsible for particle explosion. Experimentally it was observed that by the end of combustion particle temperature decreases to about  $1750^\circ\text{C}$ , what is the temperature at which many phase transformation in binary Ti-O system takes place, including eutectic  $\text{Ti}_2\text{O}_3$  formation [4]. Lower values of heat release predicted by our model can be explained by fact that we have neglected possible titanium nitrate production.

Fig. 10 presents the time variance of predicted fractions of species in  $\text{Ti}_x\text{O}_y$  vapor on droplet surface. These results explain why our model predicts heat release more accurate than theoretical predictions of Molodetsky et al. [1], who assumed that only stoichiometric titanium oxides are evaporated from the combusting particle. It was calculated that 54% of titanium mass was evaporated from particle during its combustion, but as oxygen was effectively dissolved in it, its diameter decreased only by 16%. Experiments shown even smaller diameter decrease, as nitrogen can be also dissolved in titanium.

As the residence time of products in computational (of order  $10^{-3}\text{s}$ ) area was too short to observe phenomena related to particles nucleation and aggregation the periodic boundary conditions for  $\text{TiO}_2$  vapor and particulate matter concentration were used, what is equivalent with assumption that droplet is surrounded by identical burning droplets. The calculations for nucleation and aggregation were performed for 300 ms. At this time mean primary particle diameter was found to be 23 nm, and average collision diameter of aggregate was 107 nm.

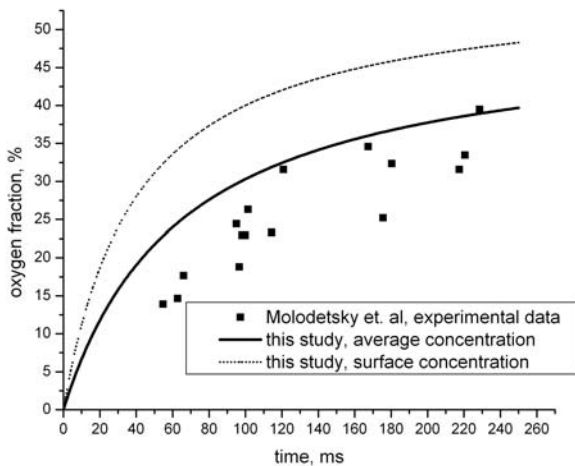


Fig. 7 History of average and surface oxygen concentration in droplet.

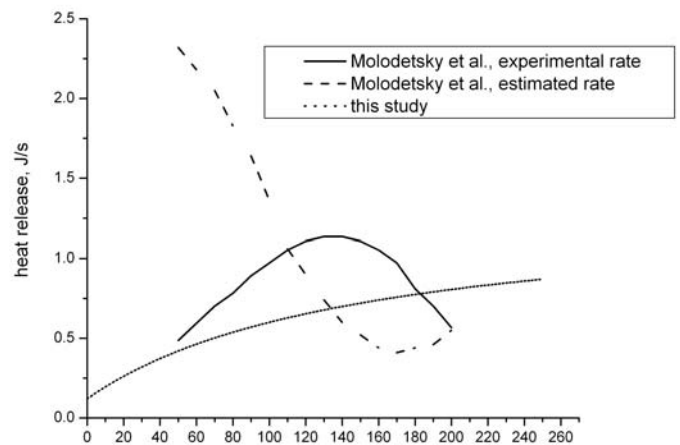


Fig. 8 Heat release of combusted droplet versus time.

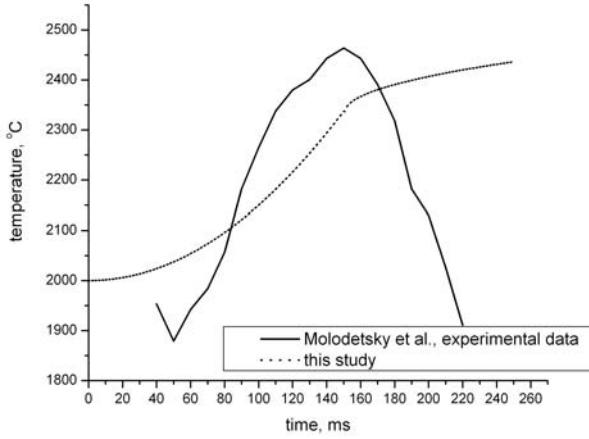


Fig. 9 Droplet's temperature history.

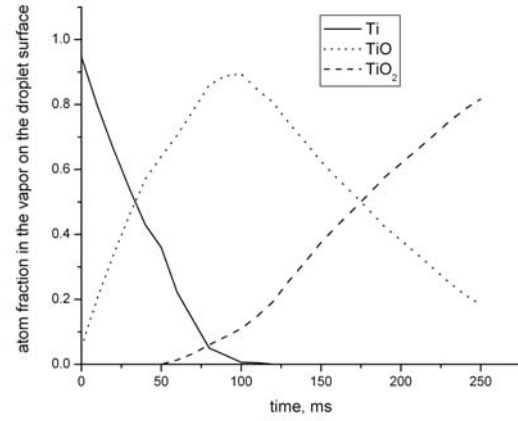


Fig. 10 Predicted species concentration at the vapor on the droplet surface

#### 4. CONCLUSIONS

The experimental results demonstrate that combustion of Al and Ti droplets results in formation of  $\text{TiO}_2$  and  $\text{Al}_2\text{O}_3$  aerosol aggregates with the size of 0.1 - 10  $\mu\text{m}$  which consist of primary particles with the diameter of 5 - 50 nm. The fractal-like dimension for these aggregates was  $D_f \approx 1.6$ . The video microscopy observations coupled with TEM analysis showed that the ratio between the equivalent geometric radius  $R$ , gyration radius  $R_g$ , mean projection radius  $R_s$  and mobility radius is  $R : R_g : R_s : R_m = 5.7 : 2.4 : 1.34 : 1$

It was found that both the ratio  $\varphi = \frac{r}{R_{\text{reac}}}$  (between the droplet radius and the radius of the reaction zone) and the radius of primary particles in  $\text{Al}_2\text{O}_3$  aggregates are functions of  $r$ . This dependences are reasonably explained by a simple diffusion model.

The combustion of Ti droplet was found to proceed via a consequence of bursts. A simple model was analysed assuming that the reason for bursts lies in the crystal shell formation followed by the nitrogen release and the droplet inner pressure increase as a consequence. Estimating the dispergation energy for the droplet as a sum of the debris kinetic energy and surface energy increase due to the newly formed surface we get the inner breaking pressure  $P_{\text{inn}} = 1.7 \times 10^5$  Pa which corresponds to the concentration nitrogen dissolved in the liquid droplet to be about 8 at. %.

We evaluated the critical supersaturation  $S_{\text{crit}} \approx 5$  for the titanium oxide vapor near the surface using a simple diffusion model. The estimations showed that the nucleation occurs at about 15  $\mu\text{m}$  from the burning surface. Then the nanoparticles are driven outwards by the thermophoresis. Very long aggregates of both  $\text{Al}_2\text{O}_3$  and  $\text{TiO}_2$  of length from a few tens to a few hundreds microns were observed which were attributed to the gelation process in the smoke tail.

In the simulation, further work is needed to explain the phenomena occurring in final stage of particle combustion. Also the possibility of co-nucleation and co-aggregation of all evaporated species should be taken into account.

## 5. REFERENCES

- [1] E. L. Dreizin. Experimental study of aluminum particle evolution in normal and micro-gravity. *Combustion and Flame*, Vol. 116, pp. 323-333 (1999).
- [2] Price E. W., Sigman R. K. Combustion of aluminized solid propellants. In: *Solid Propellant Chemistry, Combustion, and Motor Interior Ballistics* / Edited by V. Yang, T. B. Brill, Wu-Zhen Ren. Progress in Astronautics and Aeronautics, V. 185. Editor-in-Chief P.Zarchan. Publ. by AIAA Inc., Reston, VA, Ch. 2.18. pp. 663-687 (2000).
- [3] A. N. Zolotko, Ya. I. Vovchuk, N. I. Poletaev, A. V. Florko, I. S. Altman Synthesis of nanooxides in two-phase laminar flames. *Combustion, explosion, and Shock Waves*, 32 (3), 24 - 33 (1996).
- [4] T. A. Brzustowski and I. Glassman, "Vapor-phase diffusion flames in magnesium and aluminum combustion. 1. Analytical study," in: H. G. Wolfhard, I. Glassman, and L. Green (eds.), *Heterogeneous Combustion*, Academic Press, New York, pp. 75–115 (1964).
- [5] E. W. Price and R. K. Sigman, "Combustion of aluminized solid propellants," in: V. Yang, T. B. Brill, and Wu-Zhen Ren (eds.), *Progress in Astronautics and Aeronautics*, Vol. 185: *Solid Propellant Chemistry, Combustion, and Motor Interior Ballistics*, Ch. 2.18. AIAA Inc., Reston, VA, pp. 663–687 (2000).
- [6] E. L. Dreizin, Phase changes in metal combustion, *Progress in Energy and Combustion Science*, **26**, 57 - 78 (2000).
- [7] P. Bucher, R. A. Yetter, F. L. Dryer, T. P. Parr, D. M. Hanson-Parr, E. P. Vicenzi. Flame structure measurement of single, isolated aluminum particles burning in air 26th Symp.(Int.) on Combustion. The Combustion Institute, pp. 1899 - 1908 (1996).
- [8] I. E. Molodetsky, E. P. Vicenzi, E. L. Dreizin, C. K. Law, Phases of Titanium Combustion in Air. *Combustion and Flame*, **112**, 522 – 532 (1998).
- [9] V. V. Karasev, A. A. Onischuk, O. G. Glotov, A. M. Baklanov, A. G. Maryasov, V. E. Zarko, V. N. Panfilov, A.I. Levykin, K. K. Sabelfeld, Formation of charged aggregates of  $Al_2O_3$  nanoparticles by combustion of aluminum droplets in air. *Combustion and Flame*, 138, 40 – 54 (2004).
- [10] Molodetsky, I.E., E.P. Vicenzi, E.L. Dreizin and C.K. Law. "Phases of titanium combustion in air," *Combustion and Flame*, **112**, 522-532 (1998).
- [11] Heideman, S.A., T.B. Reed and P.W. Gilles "The high temperature vaporization and thermodynamics of titanium oxides" *High Temp. Sci.* **13**, 79-90 (1980).
- [12] Kazenas, E.K. and Y.V. Tsvetkov *Isparienie oxidov*, Nauka, St. Petersburg, (1997).
- [13] Massalski, T.B., H. Okamoto, P.R. Subramanian and L. Kacprzak (eds.) *Binary Alloys Phase Diagrams*, ASM Publications, Materials Park, Ohio (1990).

- [14] Waldner, P. and G. Eriksson "Thermodynamic modeling of the system titanium-oxygen" *Calphad*, **23**, 189-218 (1999).
- [15] Hobler, T. *Dyfuzyjny ruch masy i ciepla*, WNT, Warsaw (1962).
- [16] Seinfeld, J.H. and S.N. Pandis *Atmospheric Chemistry and Physics: From Air Pollution to Climate Change*, Wiley, New York (1997).
- [17] Girshick, S.L., and C.-P. Chiu "Kinetic nucleation theory: A new expression for the rate of homogeneous nucleation from an ideal supersaturated vapor" *J. Chem. Phys.* **93**, 1273-1277 (1990).
- [18] Seinfeld, J.H. *Atmospheric Chemistry and Physics of Air Pollution*, Wiley, New York (1986).
- [19] Vemury, S., K.A. Kusters, and S.E. Pratsinis "Modeling of coagulation and sintering of particles" *Proc. Int. Particle Technol. Forum, 2004*, pp. 350-356 August 17-19, Denver, USA (1994).
- [20] Kruis, F.E, K.A. Kusters, S.E. Pratsinis, and B. Scarlett "A simple model for the evolution of the characteristics of aggregate particles undergoing coagulation and sintering" *Aerosol Sci. Technol.* **19**, 514-526 (1993).
- [21] Seto, T., A. Hiroshita, T. Fujimoto, M. Shimada, and K. Okuyama "Sintering of polydisperse nanometer size agglomerates" *Aerosol Sci. Technol.* **27**, 422-438 (1997).
- [22] M.H. Peters, and Ying, R. "Phase Space Diffusion Equations for Brownian Particle Motion Near Surfaces" *Chem. Eng. Comm.*, **108**, 165-184 (1991).